Solid Earth, 12, 2553–2571, 2021
https://doi.org/10.5194/se-12-2553-2021

Solid Earth Open Access EGU

Basin inversion: reactivated rift structures in the central Ligurian Sea revealed using ocean bottom seismometers

Martin Thorwart[1], Anke Dannowski[2], Ingo Grevemeyer[2], Dietrich Lange[2], Heidrun Kopp[1,2], Florian Petersen[2], Wayne C. Crawford[3], Anne Paul[4], and the AlpArray Working Group✚

[1]CAU, Institute of Geosciences, Christian-Albrechts-Universität zu Kiel, 24105 Kiel, Germany
[2]GEOMAR, Marine Geodynamics, Helmholtz Centre for Ocean Research Kiel, 24148 Kiel, Germany
[3]IPGP, Laboratoire de Géosciences Marines, Institut de Physique du Globe de Paris, Paris, 75238 Cedex 5, France
[4]Univ. Grenoble Alpes, Univ. Savoie Mont Blanc, CNRS, IRD, UGE, ISTerre, 38000 Grenoble, France
✚For further information regarding the team, please visit the link which appears at the end of the paper.

Correspondence: Anke Dannowski (adannowski@geomar.de) and Martin Thorwart (martin.thorwart@ifg.uni-kiel.de)

Received: 29 January 2021 – Discussion started: 5 February 2021
Revised: 29 July 2021 – Accepted: 1 October 2021 – Published: 12 November 2021

Abstract. The northern margin of the Ligurian Basin shows notable seismicity at the Alpine front, including frequent magnitude 4 events. Seismicity decreases offshore towards the Basin centre and Corsica, revealing a diffuse distribution of low-magnitude earthquakes. We analyse data of the amphibious AlpArray seismic network with focus on the offshore component, the AlpArray ocean bottom seismometer (OBS) network, consisting of 24 broadband OBSs deployed for 8 months, to reveal the seismicity and depth distribution of micro-earthquakes beneath the Ligurian Sea.

Two clusters occurred between ∼ 10 km to ∼ 16 km depth below the sea surface, within the lower crust and uppermost mantle. Thrust faulting focal mechanisms indicate compression and an inversion of the Ligurian Basin, which is an abandoned Oligocene–Miocene rift basin. The basin inversion is suggested to be related to the Africa–Europe plate convergence. The locations and focal mechanisms of seismicity suggest reactivation of pre-existing rift-related structures. Slightly different striking directions of presumed rift-related faults in the basin centre compared to faults further east and hence away from the rift basin may reflect the counterclockwise rotation of the Corsica–Sardinia block. High mantle S-wave velocities and a low Vp/Vs ratio support the hypothesis of strengthening of crust and uppermost mantle during the Oligocene–Miocene rifting-related extension and thinning of continental crust.

1 Introduction

Earthquakes of magnitude 4 are frequently recorded in the Ligurian Basin, which is a plate interior. In particular, the Ligurian margin at the junction between the southwestern Alps and the Ligurian Basin (hereafter named the Alps–Liguria junction) is active with maximum magnitudes of M_w 6 to 6.5, indicating a moderate seismic activity with occasionally strong earthquakes (Béthoux et al., 1992, 2008; Courboulex et al., 2007; Larroque et al., 2012, 2016; Manchuel et al., 2017). Seismic activity is highest along the Côte d'Azur and the Ligurian coast and decreases towards the central basin and Corsica (Fig. 1). The Ligurian Sea formed during Oligocene–Miocene times as a back-arc basin (Burrus, 1984; Rehault et al., 1984; Faccenna et al., 1997; Gueguen et al., 1998; Rosenbaum et al., 2002), but extension stopped in ∼ 16 Ma. Nocquet and Calais (2004) have shown that the most of the plate convergence between Africa and Europe is accommodated at the Maghrebian chain. A present-day horizontal convergent motion of 0.4 mm yr^{-1} is observed between the Corsica–Sardinia block and mainland Europe (Nocquet, 2012; Masson et al., 2019). Compressive earthquakes occasionally occur in north-dipping reverse faults at the northern margin, indicating basin inversion (Larroque et al., 2011; Sage et al., 2011). The interior of plates is, in general, predominantly aseismic (McKenzie and Parker, 1967). In these relatively stable tectonic regions, sparse seismicity may represent diffuse deformation and is

commonly related to the reactivation of pre-existing fault planes (Zoback, 1992). In the Tyrrhenian Sea, the Africa–Europe convergence caused reactivation of pre-existing fault planes, revealing an inversion of the basin that is mainly observed along the margins (Zitellini et al., 2020).

Here, we report on local seismicity in the centre of the Ligurian Basin (Fig. 1a). We analysed two earthquake clusters (Fig. 1b) that were recorded by an amphibious seismic network operated in the framework of the European AlpArray initiative (Hetényi et al., 2018). The AlpArray ocean bottom seismometer (OBS) network, a long-term broadband OBS array, recorded ground motion continuously for eight months (June 2017–February 2018). The long-term OBS deployment enables robust source estimates of earthquakes far away from land stations. Nevertheless, observations from the land stations improved the estimate of fault plane solutions. The observed earthquake clusters and their depth distribution provide constraints on the crust and upper mantle rheology and provide insights into the current regional stress field.

2 Geological and geodynamic setting

The western Mediterranean, including the waters west of Apennines and Sicily, consists of several basins (Fig. 2) that formed from Oligocene–Miocene times to the present (e.g. Burrus, 1984; Rehault et al., 1984). The geodynamic setting was controlled by the convergence of the African and Eurasian plates (e.g. Dercourt et al., 1986; Nocquet and Calais, 2004; Serpelloni et al., 2007) and the rollback of the Apennines, Calabrian and Gibraltar subduction zones (Jolivet and Faccenna, 2000). The fast rollback of the westward-migrating Gibraltar arc and the south-eastward-retreating Apennines-Calabrian arc played a major role in the opening of the Mediterranean sub-basins (Frizon de Lamotte et al., 2000; Mauffret et al., 2004; Handy et al., 2010). The Ligurian Basin, opening in $\sim$ 30–16 Ma (Burrus, 1984; Bache et al., 2010), and the Alboran Basin, opening in $\sim$ 27–8 Ma (Comas et al., 1999), are the oldest basins in the western Mediterranean. The Algerian Basin, opening in $\sim$ 16–8 Ma (Mauffret et al., 2004), and the Tyrrhenian Basin, opening in $\sim$ 8–0 Ma (Faccenna et al., 2001, 2004; Rosenbaum et al., 2002), are the youngest basins in the western Mediterranean. In the latter two basins, geophysical and geological data clearly show that extension caused break-up and seafloor spreading (Nicolosi et al., 2006; Bouyahiaoui et al., 2015; Prada et al., 2016; Booth-Rea et al., 2018), while the Alboran Basin is a domain of extended continental crust modulated by arc magmatism (Booth-Rea et al., 2018; Gómez de la Peña et al., 2020). The SW part of the Liguro-Provençal Basin is floored by "atypical" oceanic crust (Gailler et al., 2009; Afilhado et al., 2015; Moulin et al., 2015). However, the extent and nature of the oceanic domain towards the north-east into the Liguro-Provençal Basin remains debated.

The Ligurian Basin underwent a long-lasting phase of extension from the Late Oligocene to Miocene (Rehault et al., 1984; Gueguen et al., 1998; Finetti et al., 2005), progressively opening from south to north with a high synrift sedimentation (Sage et al. (2011). Based on magnetic and seismic data, oceanic spreading with unroofing of mantle material was proposed for the late opening period $\sim$ 21–16 Ma (Le Douaran et al., 1984; Pascal et al., 1993; Contrucci et al., 2001; Rollet et al., 2002; Speranza et al., 2002). For the Ligurian Basin, which is the NE part of the Liguro-Provençal Basin, a recent analysis of a seismic refraction profile proposes that rifting failed before oceanic spreading initiated, while it remains unclear if mantle was exhumed or an extreme thin layer of continental crust remained (Dannowski et al., 2020). The analysis of a seismic refraction study along a profile from the northern margin to the basin centre (Dessa et al., 2020) might shed further light on the crustal structure. The Corsica–Sardinia block underwent a counter-clockwise (CCW) rotation (Alvarez et al., 1973; Rehault et al., 1984; Speranza et al., 2002; Maffione et al., 2008) of $\sim$ 23° (Speranza et al., 2002) to 45° (Gattacceca et al., 2007) between $\sim$ 21–16 Ma, and of 53° between 35–16 Ma (Le Breton et al., 2017), with an Euler rotational pole near Genoa, onshore or in the Gulf of Genoa (Fig. 2). Extension in the Ligurian Basin ended in $\sim$ 16 Ma and continued afterwards in the Algerian and Tyrrhenian basins (Mauffret et al., 2004).

The Calabrian trench retreats further south-eastwards (Fig. 2, white arrow), but recent seismological observations indicate that Tyrrhenian Sea opening slowed down or ceased and the Africa–Eurasia convergence results in basin inversion at its southern rim (Zitellini et al., 2020). It is proposed that the major shortening caused by the convergence between Africa and Europe is currently accommodated in the Maghrebides ranges in northern Africa (90 %–100 %) and that the Ligurian Basin and the Corsica–Sardinia block are rigid (Nocquet and Calais, 2004; Béthoux et al., 2008; Nocquet, 2012). However, passive seismic studies observe signatures of compression in the Ligurian Basin (Béthoux et al., 1992, 2008; Baroux et al., 2001; Eva et al., 2001; Courboulex et al., 2007; Larroque et al., 2011, 2012, 2016). The main portion of the compression is accommodated in active north-dipping reverse faults at the Ligurian margin proposed to be active since $\sim$ 5 Ma (Béthoux et al., 2008; Sage et al., 2011; Larroque et al., 2011). The Ligurian margin was uplifted by more than 1 km with respect to the basin (Sage et al., 2011; Larroque et al., 2011). Moreover, active compressional structures were imaged in seismic reflection profiles (Bigot-Cormier et al., 2004) off the Ligurian coast. Along the Corsica margin, seismic reflection data do not image significant faults that reached the surface in the last $\sim$ 5 Myr, but earthquakes of M_L 5.5 and 4.4 occurred in July 2011 off the coast of Corsica (Larroque et al., 2016) (Fig. 1, grey star). The low seismicity in the central basin and in the southern part off the coast of Corsica indicate a weaker and more recent deformation (Béthoux et al., 2008; Larroque et al., 2016), while

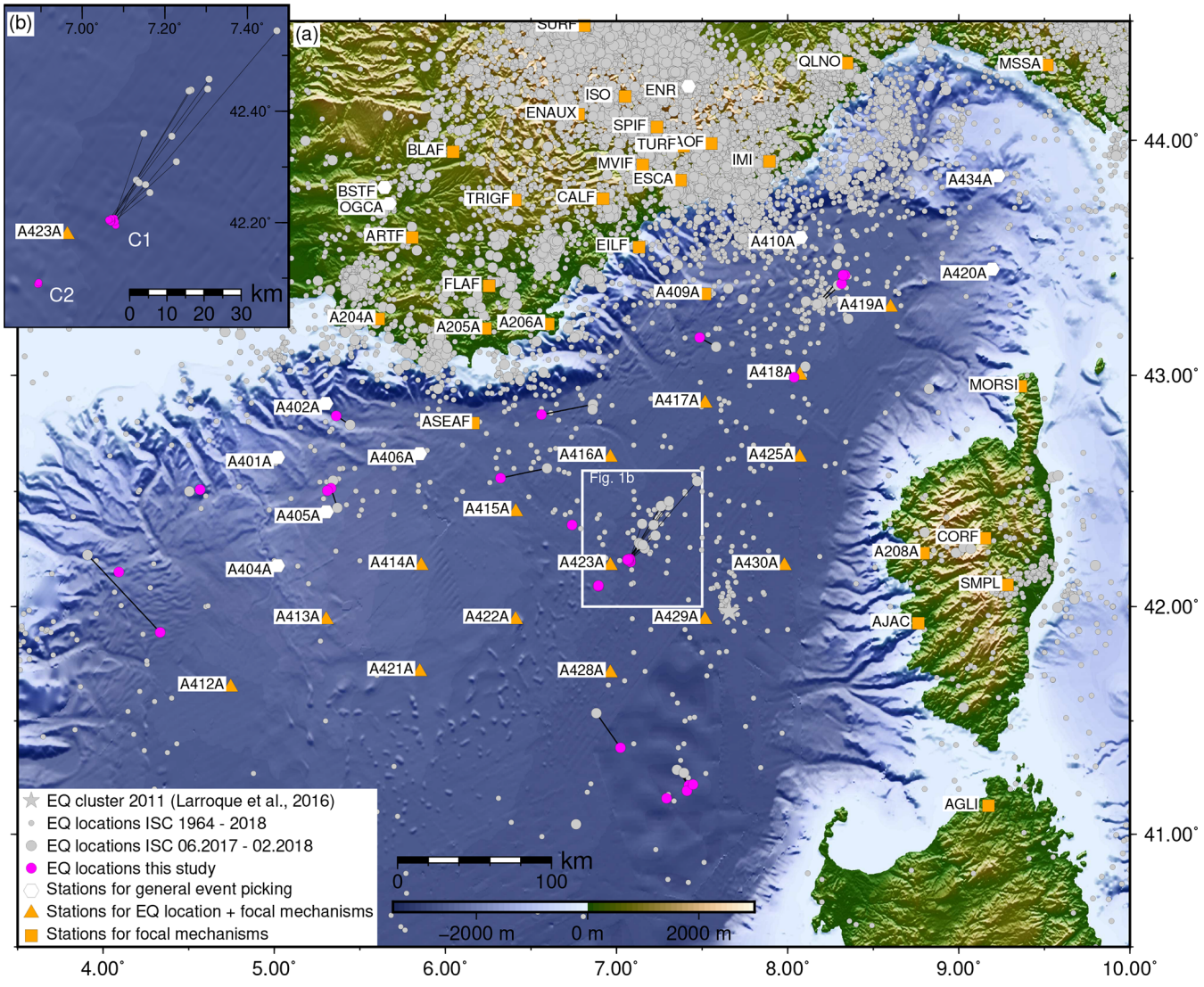

Figure 1. Topographic map of **(a)** the Ligurian Sea and **(b)** the area where the cluster events occurred (GMRT data, Ryan et al., 2009). Grey circles mark the epicentres of earthquakes from the ISC bulletin (Storchak et al., 2017). Magenta circles mark the epicentres of earthquakes within the Ligurian Basin observed in this study. Black lines connect locations of the same events found in both the ISC bulletin and this study.

the Ligurian margin is narrow and steep with a few listric normal faults, the Corsica margin is wider and several listric faults were imaged in seismic reflection data (Finetti et al., 2005). Within a short distance of 30–50 km, the crust–mantle boundary (CMB) deepens from ∼ 15 km depth in the basin to ∼ 25 km depth at the continental margins (Contrucci et al., 2001; Gailler et al., 2009; Dessa et al., 2011).

3 Data and results

The AlpArray OBS network consisted of 24 broadband OBSs (Fig. 1) that continuously recorded ground motion for ∼ 8 months (June 2017 to February 2018). The stations were deployed with a spacing of ∼ 60 km using the French research vessel *Pourquoi Pas?* and recovered during research cruise MSM71 on the German research vessel *Maria S. Merian*. Data from two OBS instrument types were used in our study: (1) a German OBS, provided by the DEPAS pool (Schmidt-Aursch and Haberland, 2017) and GEOMAR (Lobster type), equipped with a Trillium Compact 120 s seismometer and an HTI-04-PCA/ULF hydrophone recording on 6D6 KUM recorders with a sampling frequency of 250 Hz, and (2) a French OBS, provided by the IPGP-INSU pool (BBOBS), equipped with a Trillium 240 s seismometer (T240) and a differential pressure gauge (DPG) recording at a frequency of 62.5 Hz. Additionally, land data (Fig. 1) were used from different regional permanent and

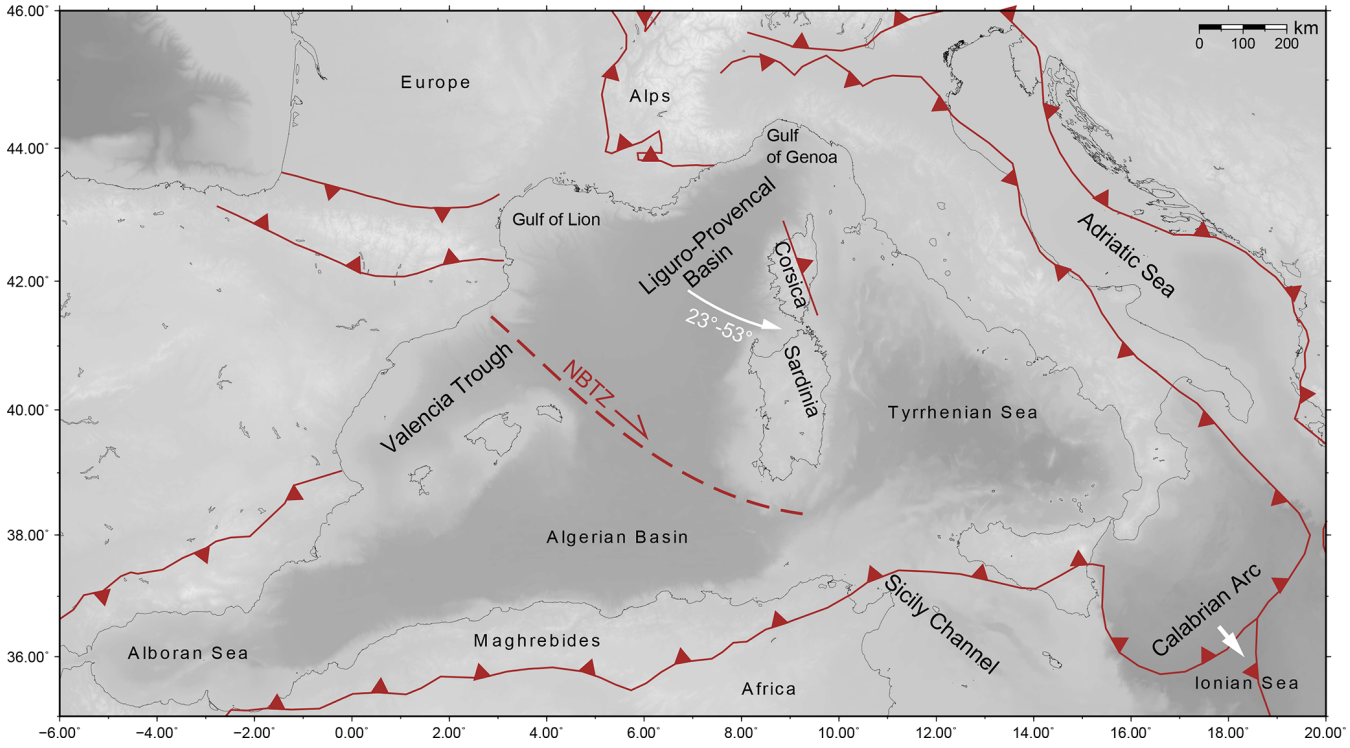

Figure 2. Geographic and tectonic overview map with thrusts modified from Le Breton et al. (2020) and the North Balearic Transform Zone (NBTZ) (van Hinsbergen et al., 2014). The white arrows indicate the ∼ 23 to 45° CCW rotation of the Corsica–Sardinia block during Miocene times (Speranza et al., 2002; Gattacceca et al., 2007) and the ∼ 53° during Oligocene–Miocene times (Le Breton et al., 2017) and the trench retreat of the Calabrian Arc. GMRT data were used as background topography (Ryan et al., 2009).

temporary seismological networks: AlpArray (Z3), Italian National (IV), French RESIF-RLBP (FR) and Mediterranean MedNet (MN).

3.1 Events, picking and location

During the long-term OBS deployment, 39 seismic events were detected within the Ligurian Basin excluding the Alps–Liguria junction zone (Fig. 1a, magenta circles). Our work focuses on two earthquake clusters in the centre of the Ligurian Basin, near OBS A423A (magenta circles in Fig. 1b; Table 1). The first cluster (C1) consists of 13 events that occurred from June to November 2017 (Fig. 3a, blue bars). The second cluster (C2) consists of three events that occurred during one day in January 2018, about 25 km south-west of C1 (Fig. 3a, red bars). Two events (grey bars in Fig. 3a) had few observations and high uncertainties; these were not used in this interpretation. Two low-magnitude events were only observed at station A423A using the template matching method (e.g. Shearer, 1994) and were not further analysed (Fig. 3a, black bars). We show that a seafloor network can detect more events than those in the land-based ISC catalogue (Table 1), whose magnitude of completeness is 2.2 in the region, but the four non-located events (grey and black bars in Fig. 3a) indicate that the AlpArray OBS station spacing is too large to render a precise picture of the local seismicity.

We first used the ISC bulletin (Storchak et al., 2017) to identify seismic events in the AlpArray OBS data. The phases were picked manually on all stations plotted with orange triangles, orange squares and white hexagons in Fig. 1b. Only the seismometer components were used in our analysis since the signal–noise ratio on most of the hydrophones was too low to identify local seismic events.

Three onsets predominated the observed events: the P wave, a converted Ps wave and the S wave (Fig. 3b, A1). The P wave is weak in amplitude and followed by a stronger Ps phase, which was observed on all OBS stations but not on land stations. S-wave amplitudes are increased by the seafloor itself due to the high impedance contrast. Additionally, the presence of a high- or low-velocity sedimentary layer with a high impedance contrast in the basin influences the wave field energy. This would only affect signals travelling through this layer, for example Messinian salts, towards the OBS and does not influence signals recorded on land stations. Because of these observations we use mainly amplitudes from land stations to estimate the fault plane solutions. Both phases indicate an apparent P-wave velocity (Vp) of $\sim 8.1\,\mathrm{km\,s^{-1}}$, and they are separated by a nearly constant time difference of ∼ 1 s. The S-wave phase has a high am-

Table 1. Epicentral locations and focal depths (with uncertainties of the relative depths) for the cluster events from HypoDD (depth below sea surface). Abbreviations: C – cluster; WFF – waveform family; F – family.

Event ID	Date	Time of origin	Latitude	Longitude	Depth (km)	Magnitude (M_L)	ISC bulletin ID	C / WFF
1	18 Jun 2017	20:55:29.48	42.194983 ± 0.0020	7.081169 ± 0.0020	10. 4 ± 0.2	1.2	610697551	C1/-
2	20 Jun 2017	17:09:51.36	42.203548 ± 0.0015	7.078639 ± 0.0015	15.5 ± 0.5	2.5	610697576	C1/F1
3	21 Jun 2017	02:28:07.10	42.207711 ± 0.0037	7.077632 ± 0.0016	15.1 ± 0.7	1.2	610779982	C1/F1
4	22 Jun 2017	08:06:29.84	42.201794 ± 0.0017	7.079651 ± 0.0015	14.9 ± 0.6	1.4	610780001	C1/F1
5	25 Aug 2017	02:19:23.09	42.202787 ± 0.0022	7.069184 ± 0.0047	16.3 ± 0.4	1.3	611003163	C1/F2
6	25 Aug 2017	02:33:43.42	42.202987 ± 0.0013	7.071468 ± 0.0015	16.1 ± 0.4	2.1	611003164	C1/F2
7	26 Aug 2017	02:26:50.22	42.202734 ± 0.0018	7.065569 ± 0.0021	15.2 ± 0.6	0.9	611003237	C1/F2
8	26 Aug 2017	02:30:33.03	42.201440 ± 0.0014	7.069776 ± 0.0015	16.1 ± 0.4	1.9	611003238	C1/F2
9	26 Aug 2017	17:31:51.84	42.202738 ± 0.0014	7.070272 ± 0.0015	16.3 ± 0.4	1.9	610933407	C1/F2
10	27 Aug 2017	00:39:30.31	42.200989 ± 0.0023	7.069771 ± 0.0042	16.0 ± 0.4	1.3	611003290	C1/F2
11	29 Aug 2017	11:54:17.80	42.1850 ± 0.047	7.1040 ± 0.092	8.4 ± 2.9	1.1		-
12	13 Sep 2017	07:47:16.31	42.205314 ± 0.0015	7.065561 ± 0.0015	16.5 ± 0.4	1.3		C1/F2
13	13 Sep 2017	09:26:57.97	42.207292 ± 0.0019	7.069896 ± 0.0017	15.9 ± 0.4	1.2		C1/F2
14	10 Nov 2017	23:05:48.52	42.204736 ± 0.0014	7.064332 ± 0.0016	14.4 ± 0.5	1.3	611617247	C1/-
15	21 Nov 2017	11:45:24.00	42.2080 ± 0.034	6.8180 ± 0.046	6.0 ± 5.2	0.9		-
16	24 Jan 2018	05:11:25.24	42.089022 ± 0.0054	6.894502 ± 0.0050	9.9 ± 0.8	1.4		C2/F3
17	24 Jan 2018	07:35:48.27	42.089233 ± 0.0046	6.892409 ± 0.0074	9.9 ± 1.7	1.4		C2/F3
18	24 Jan 2018	09:43:10.11	42.091915 ± 0.0062	6.894325 ± 0.0051	10.5 ± 2.0	1.2		C2/F3

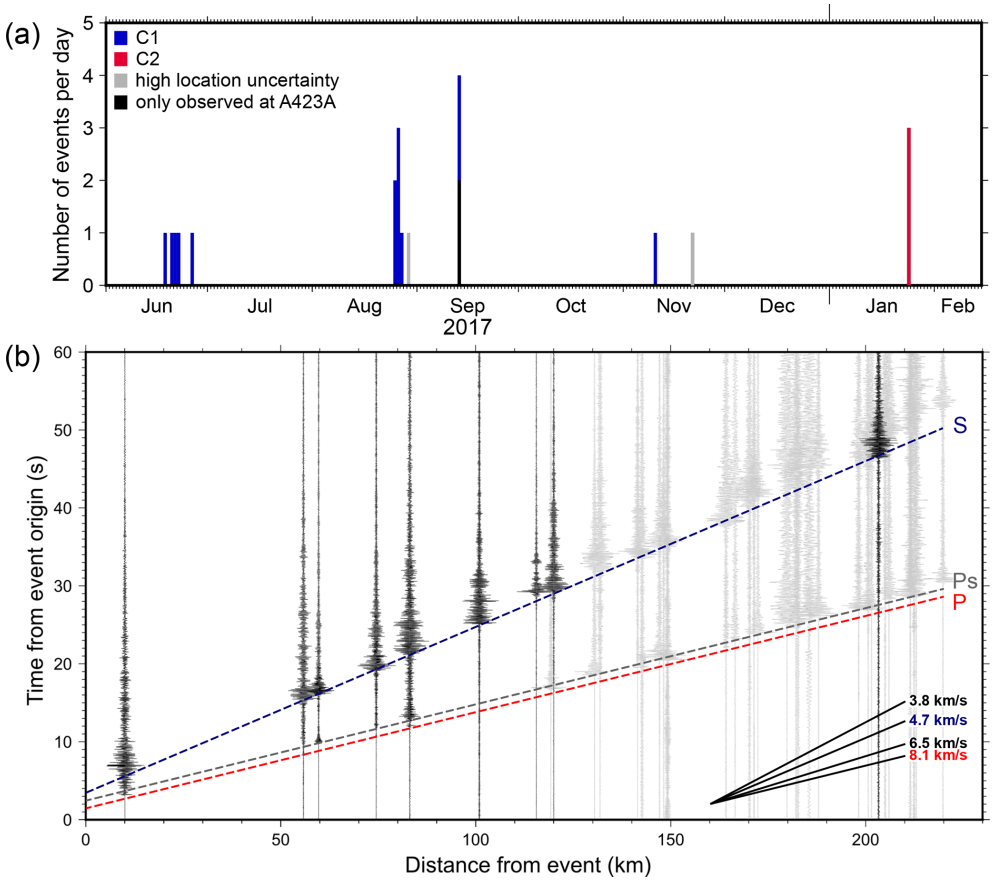

Figure 3. Panel **(a)** shows the temporal development of the cluster events in blue for C1 and in red for C2. Black events were only observed at A423A and not further analysed. Grey events were located with high uncertainties. **(b)** Waveforms of the strongest event of C1 (20 June 2017) displayed over offset. Black traces were used for EQ location. A weak P onset (red line) is observed, followed by a stronger Ps phase (grey line) ∼ 1 s later. The S phase (blue line) is clearly visible at all stations. Apparent velocities of Vp = 8.1 km s^{-1} and Vs = 4.7 km s^{-1} are observed for the phase onsets (marked with dashed lines). More examples in Appendices (Fig. A1).

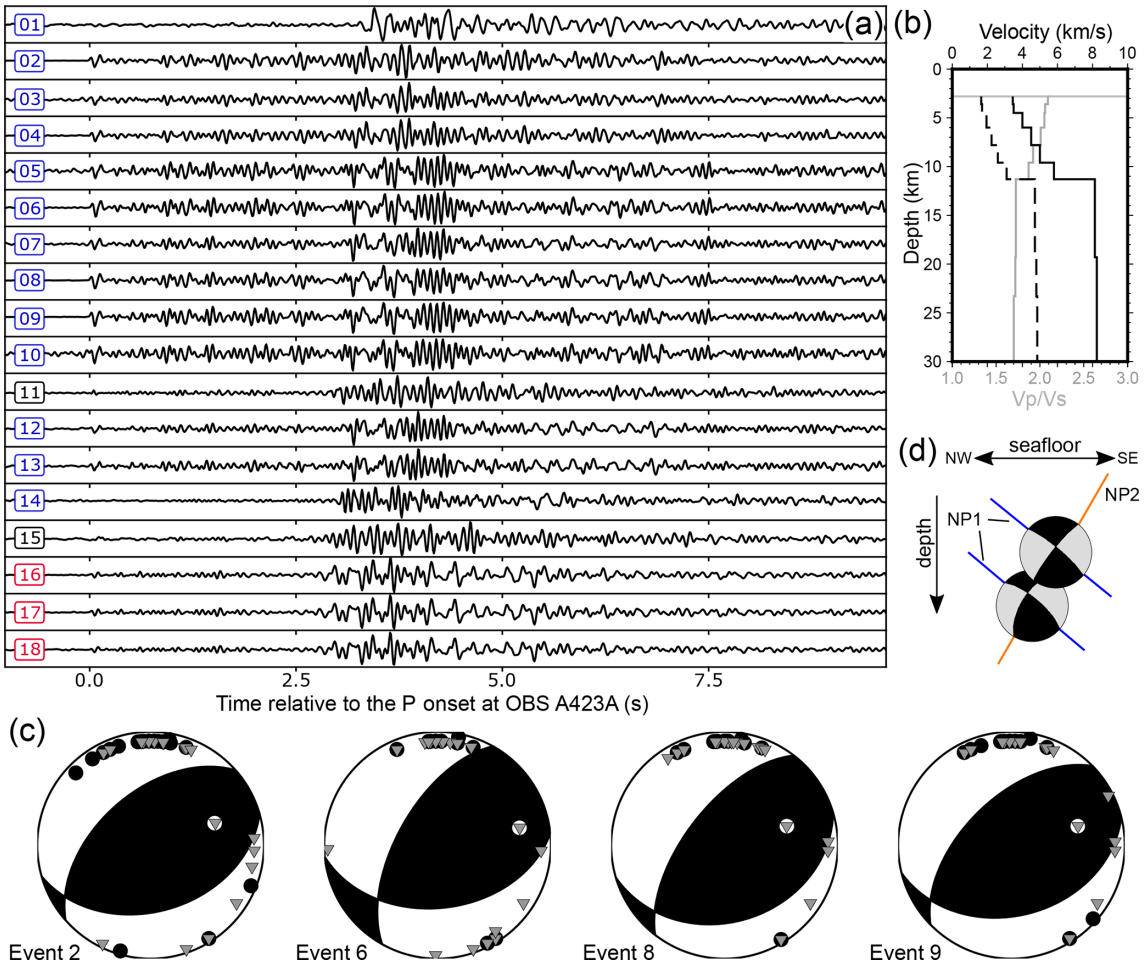

Figure 4. **(a)** All observed cluster events recorded at station A423A, Z component (bandpass filtered 2–20 Hz). The P onsets are shifted so that they align at 0 s. **(b)** 1-D velocity models (Vp, solid line, Vs, dashed line, and Vp/Vs grey solid line) used to relocate the cluster events. **(c)** Focal mechanisms of events 2, 6, 8 and 9, computed using the amplitude ratio of Sv/*P* (grey inverted triangles) and the wave polarisation (black dots for negative polarisation) determined at OBS and land stations. **(d)** Sketch of the two nodal planes (NP) of events 2 (upper) and 6 (lower) as side view.

plitude, compared to the P onsets, and shows an apparent S-wave velocity (Vs) of $\sim 4.7\,\mathrm{km\,s^{-1}}$ (Fig. 3b). The waveforms are highly coherent as shown for the vertical component of station A423A (Fig. 4a). We picked the P onset on the vertical component and the S onset on the horizontal components using SEISAN (Havskov and Ottemoller, 1999).

Within cluster C1, two main waveform families (WFFs) are observed, indicating a repeated activation of the fault. Family 1 (F1) was active in June 2017 and consists of events 2, 3 and 4. Family 2 (F2) was active at the end of August and again in September 2017 and consists of events 5 to 10, 12 and 13. Cluster C2 consists of a third waveform family (F3), events 16 to 18. The coherency within the families is > 0.8.

We use only stations within the basin (orange triangles in Fig. 1) to locate the events. In this way, we can use a 1-D seismic velocity model for the basin and avoid errors introduced by the extreme topography and changes in crustal thickness near the margins. The determination of the absolute depths was challenging, since the stations show only Pn and Sn phases, except for OBS A423A, which was close enough to observe Pg/Sg and Pb/Sb phases. We applied a 1-D velocity model (Fig. 4b) based on P-wave velocities from seismic refraction profile p02 (Dannowski et al., 2020) (Fig. 5e). A Vp/Vs ratio of 2.0 at the seafloor and 1.87 above the CMB was assumed to calculate Vs (Fig. 4b). The observed apparent velocities of mantle refracted waves Pn and Sn (Fig. 3b) were used as Vp and Vs for the uppermost mantle in the 1-D velocity models (Fig. 4b). First, an initial event location using HYPOCENTER (for event location) and RMSDEP (for uncertainties of absolute depths, Fig. A2) routines within SEISAN (Havskov and Ottemoller, 1999 and references therein) was done. Afterwards, events of the two clusters were relocated with HypoDD, a double-difference

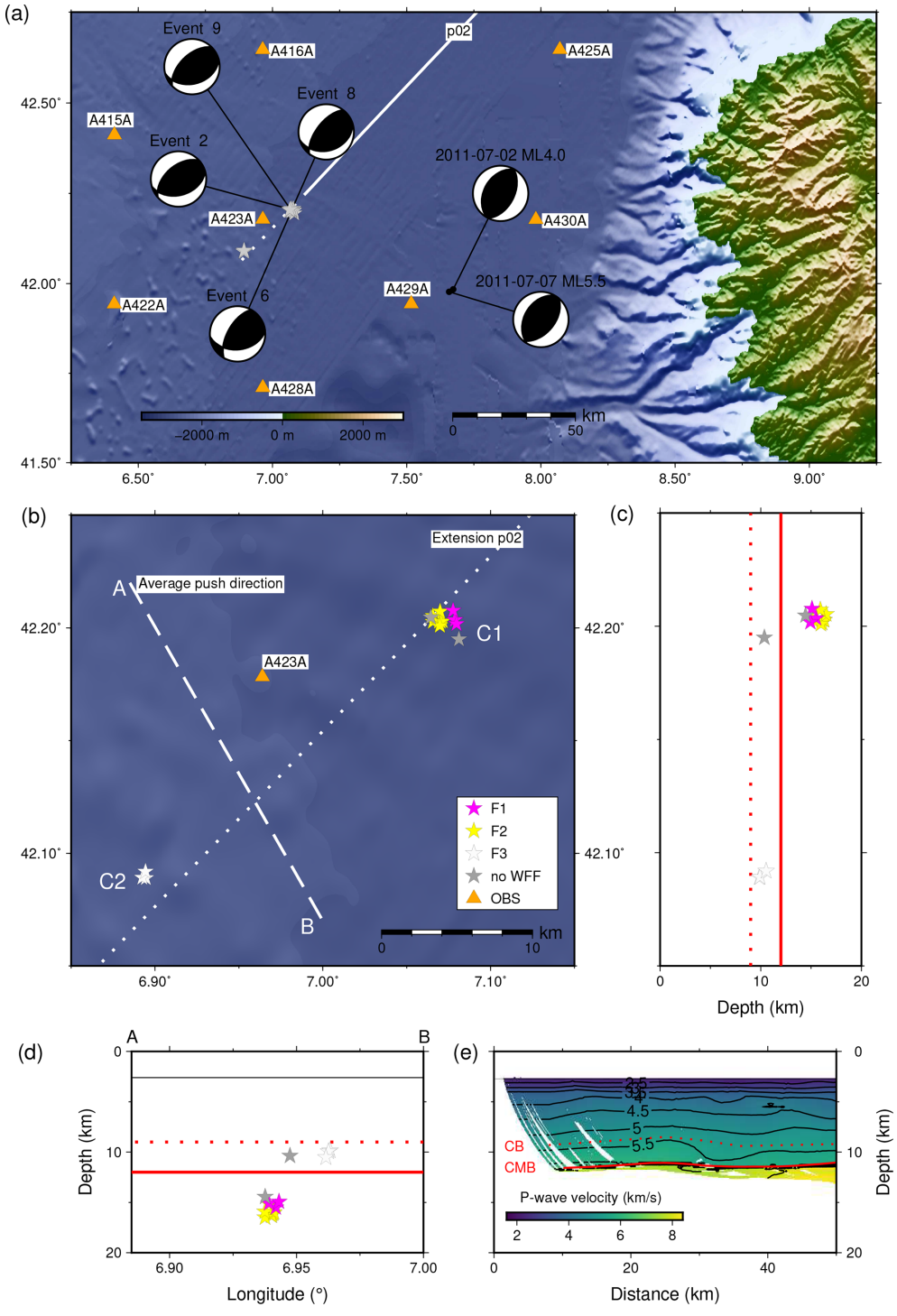

Figure 5. **(a)** Focal mechanisms of C1 cluster and two events in 2011 (Larroque et al., 2016). **(b)** Close-up of the map from panel **(a)**. The white dotted line indicates the prolongation of seismic refraction profile p02 (white line in panel **a**) and the white dashed line represents the main horizontal direction of the pressure axis P as indicated by focal mechanisms. Events are displayed coloured according to their wave form family (WWF). **(c)** Depth distribution of the cluster events from north to south. **(d)** Events projected on the dashed line A–B shown in panel **(b)**. The thin black line indicates the seafloor, the dotted red line is the base of the sediment layers (CB) and the solid red line is the crust–mantle boundary (CMB). **(e)** SW end of the seismic velocity model computed from seismic refraction profile p02 (Dannowski et al., 2020). Topography from GMRT data (Ryan et al., 2009).

earthquake algorithm for relative relocations (Waldhauser and Ellsworth, 2000). Because our clusters contain only a few events and the background velocity model is well-constrained, we used HypoDD's singular value decomposition (SVD) solver. All events of F1 and F2 (cluster C1) are located in the uppermost mantle (between 15 and 17 km depth), while the events of F3 (cluster C2) are located in the crust. This is supported by observations at station A423A, where Pg/Sg phases could be observed for the events of F3 but not for the events of F1 and F2. Further plots on the accuracy of the focal depths are given in the Appendices (Fig. A2).

We compared epicentres of events observed in both the ISC bulletin and our study. Pairs are connected by black lines in the seismicity map (Fig. 1). The epicentres based on the ISC bulletin are spread over a 50 km × 20 km zone, whereas the same events located solely using OBS data lie in a very narrow 3 km × 3 km zone (Figs. 1b and 5b). Additional events with magnitude $M_L < 2$ were detected using the OBS; these events were also recorded by the land stations (Fig. 1), but their amplitudes were close to the noise level.

3.2 Focal mechanisms

To estimate fault plane solutions, we used the stations shown in orange in Fig. 1, plus the permanent station VSL in southern Sardinia (located outside the map of Fig. 1a). The station distribution provided a good azimuthal coverage for the Ligurian Sea. The first motion direction of the P wave was determined for on- and offshore stations where clearly visible (examples in Fig. A3). The amplitude ratio of P to S waves was determined on the vertical component at land stations only. The amplitudes were corrected for attenuation effects using $Q_s = 600$ and $Q_p = 1300$ in the program FOCMEC (Snoke, 2003). The ocean bottom stations showed unusually small amplitudes for the P wave compared to the S wave, indicating a low velocity contrast between sedimentary layers and water and suggesting a low subsurface shear modulus. Together with the high instrument mass, these effects could not be taken properly into account to determine amplitude ratios of P to S waves for the OBS. Polarity (Fig. A3) and amplitude ratios (Fig. A4) were used to derive the fault plane solution of events 2, 6, 8 and 9 (Fig. 4c; Table 2) using the program FOCMEC (Snoke, 2003). Strike directions and their uncertainties are presented in Fig. 4c. The uncertainties result from a systematic grid search for polarity and amplitude ratios using FOCMEC. Afterwards, the 20 best possible solutions for each event were averaged and the standard deviation was calculated (Table 2). In general, the events of cluster C1 show stronger amplitudes compared to C2. The four fault plane solutions of cluster C1 indicate thrust faulting (Figs. 4c and 5a). The arrivals from events of C2 were not of sufficient quality to calculate focal mechanisms.

4 Discussion

4.1 Basin inversion

Geodetic measurements in Corsica and Sardinia show residual velocities $< 0.5\,\mathrm{mm\,yr^{-1}}$ with respect to stable Europe (Nocquet and Calais, 2004), which the authors use to conclude that the shortening at the Alps–Liguria junction, expressed in widely distributed low- to moderate-magnitude earthquakes, is a result of the ongoing CCW rotation of the Adriatic microplate, rather than a S–N motion of the Corsica–Sardinia block. Furthermore, Larroque et al. (2016) observed an earthquake cluster in 2011 off the coast of Corsica (Fig. 5a) accompanied by events in 2012 and 2013 located in the same area, but they did not observe surface ruptures or faults rupturing the Plio–Quaternary sediments in the epicentre area of the 2011 events.

Inspired by their analysis, we studied the seafloor bathymetry in the C1 and C2 regions, but we did not observe any fault structures, and pre-existing multi-channel seismic data did not reveal sufficiently large faults in the sedimentary strata. There remains uncertainty on the depth of the base of the sediment layers from the refraction seismic study (Fig. 5e) (Dannowski et al., 2020); however, the C1 and C2 events are smaller than the 2011 events and occurred at similar focal depth. Thus, we assume that the rupture areas are entirely located within the lower crust and uppermost mantle and do not reach post-rift sediments. This suggests a long-term deformation without accumulating slip concentrated in one fault plane but rather distributed rupture areas. C1 consists of two waveform families indicating repeated activation of the same fault plane for events of the same family. Events of one family have very similar waveforms (Fig. 4a) because they originate from the same fault plane. Events of family 2 occur at greater depth than events of family 1. We observe two possible nodal planes with a main strike in the NE–SW to ENE–WSW directions (Fig. 4c and d, Table 2). However, we cannot identify which of the two was activated. For the second nodal plane (NP2, Fig. 4d) the event locations and the direction of the nodal plane coincide, indicating that the same fault was activated at different depths. For the first nodal plane (NP1, Fig. 4d) the events would have occurred on two neighbouring faults. The same is true for the relationship between C1 and C2, where we observed a third waveform family. Based on the data we cannot conclude if the clusters C1 and C2 belong to one fault or to two separate nearby faults; therefore we use the term "rupture area".

Larroque et al. (2016) debated whether the 2011 cluster resulted from ridge-push forces of an oceanic spreading centre in the Ligurian Basin or a southward propagation of the deformation at the Alps–Liguria junction. They exclude the hypothesis of a spreading centre, since no spreading axis had been mapped. Our study corroborates this hypothesis, since clusters C1 and C2 are located in the basin centre and would be even closer to or at the proposed spreading

Table 2. Fault plane solution for events 2, 6, 8 and 9.

Event ID	Date	Time of origin	Plane 1			Plane 2		
			Strike	Dip	Rake	Strike	Dip	Rake
2	20 Jun 2017	17:09:51.36	$74 \pm 5°$	$41 \pm 2°$	$110 \pm 5°$	$229 \pm 5°$	$52 \pm 2°$	$74 \pm 4°$
6	25 Aug 2017	02:33:43.42	$84 \pm 4°$	$43 \pm 2°$	135 ± 5	$210 \pm 4°$	$62 \pm 3°$	$57 \pm 4°$
8	26 Aug 2017	02:30:33.03	$73 \pm 29°$	$33 \pm 10°$	$121 \pm 9°$	$217 \pm 25°$	$63 \pm 9°$	$71 \pm 8°$
9	26 Aug 2017	17:31:51.84	$76 \pm 12°$	$38 \pm 7°$	$114 \pm 17°$	$226 \pm 13°$	$57 \pm 9°$	$73 \pm 8°$

axis, and so ridge-push forces would be higher. Additionally, no spreading axis was mapped in previous seismic studies that interpreted the nature of the basin centre as "atypical" oceanic crust (Contrucci et al., 2001; Rollet et al., 2002). Analysis of the LOBSTER seismic refraction profile p02 (Dannowski et al., 2020) proposes that rifting failed before seafloor spreading was initiated.

The driving mechanism for the deformation of the Ligurian basin has to be searched outside the basin. To summarise previous studies, sources for the regional compressional stresses in the basin centre could be (1) Africa–Europe convergence, (2) CCW rotation of the Adriatic plate (Larroque et al., 2016) or (3) north-eastward motion of the Tyrrhenian Sea towards stable Europe (Nocquet, 2012). The geodetic network lacks stations in northern Africa, excluding reliable geodetic constraints on plate motions (Nocquet, 2012).

The latest plate motion models (Nocquet, 2012) are based on seismicity and other geophysical and geological information and indicate that the majority (90 %–100 %) of Europe–Africa convergence is accommodated in the Maghrebides. An analysis of two decades of dense GPS data presents a $\sim 0.4\,\mathrm{mm\,yr^{-1}}$ motion of Corsica representing a NNW–SSE shortening that is compatible with the tectonic and seismicity observations at the Ligurian margin (Masson et al., 2019), while Eva et al. (2020) show in a seismic study that the CCW rotation of the Adria block has no influence south of 45° N.

The epicentres of cluster C1 were located in the uppermost mantle (one event in the lower crust) and their mechanisms are thrust faulting (Fig. 5), while the epicentres of cluster C2 were located in the lower crust, above the CMB. The 2011 events were also thrust faulting events which occurred in the crust and uppermost mantle (Larroque et al., 2016), roughly 50 km E-SE of clusters C1 and C2. If we project C1 and C2 on line A–B that follows the push direction (based on the rake, Table 2) of the thrust events, they map in a slightly tilted vertical plane dipping north-westwards (Fig. 5d). Independently of the source of regional stresses, we interpret the C1 and C2 clusters and the 2011 cluster as a result of basin inversion and hence a reactivation of the Oligocene–Miocene rift-related structures. The main portion of the basin inversion in the Ligurian Basin is accommodated at the northern margin where a high rate of seismicity is observed compared to the basin centre and the Corsican margin (Béthoux et al., 2008). Active northward-dipping reverse faults have been mapped that are evidence for a 5 Myr cumulative deformation with a margin uplift of more than 1 km (Larroque et al., 2011, Sage et al., 2011). The centre of the Ligurian Basin and the Corsican margin are characterised by low seismicity and diffuse distribution of rupture areas of small size spread over a wide area, which indicates the absence of cumulated deformation and points to a weaker or more recent deformation (Larroque et al., 2016). Shortening in the Ligurian Basin could reactivate these pre-existing rift-related structures, suggesting ongoing closure of the Ligurian Basin. Our results show that seismicity based on land stations underestimates the number of earthquakes in the Algerian and Ligurian basins. Reactivation of pre-existing and often rifting-related fault planes was observed in other areas, for example in the Tyrrhenian Sea (Zitellini et al., 2020); in the Gulf of Cadiz (Grevemeyer et al., 2016); and in northern Honshu, Japan (Kato et al., 2009). Therefore, like the Tyrrhenian Sea (Zitellini et al., 2020), the Ligurian Sea may have entered a stage of basin inversion.

4.2 Orientation of pre-existing rift-related faults

While earthquakes are spread over the entire Ligurian Basin (Fig. 1), the C1 and C2 events cluster within small areas. C1 and C2 are separated by ~ 25 km in a NE–SW direction. It is possible that both clusters may originate from the same fault zone; however, this cannot be clearly determined by our dataset. The focal mechanisms of cluster C1 are similar to the 2011 events (Larroque et al., 2016). We observe a difference in the average striking direction of $\sim 40°$ for the first nodal planes and $\sim 10°$ for the second nodal plane of C1 (WSW–ENE to SW–NE) compared to the striking direction of the 2011 events (SW–NE to SSW–NNE). As discussed before, we interpret the three clusters as caused by the reactivation of Oligocene–Miocene rift-related structures. Normal faults that were created during the extensional phase are inverted into reverse faults and their strikes are those of the normal faults during the extensional phase. Thermo-mechanical modelling suggests that rifting-related structures get younger oceanwards (Brune et al., 2014). Since the structures supported by the 2011 events are located more to the south-east, i.e. closer to the coast, they represent early rifting stage structures, whereas the structures supporting C1 and C2, located

more to the centre of the basin, were developed during a later rifting stage. Thus, we speculate that this difference in strike ($\sim 10°$ or $\sim 40°$) might be connected to the CCW rotation of the Corsica–Sardinia block compared to stable Europe that was estimated in previous studies with $\sim 23°$ (Speranza et al., 2002) to $\sim 45°$ (Gattacceca et al., 2007) between 21–16 Ma or 53° between $\sim$ 35–16 Ma (Le Breton et al., 2017) in total amount of rotation.

4.3 Rheology of crust and uppermost mantle

The occurrence of C1 at mantle depths and a high S-wave velocity combined with a low Vp/Vs ratio are puzzling. Earthquakes in continental domains normally occur in the upper crust, while the lower crust is relatively aseismic, and earthquakes are rare in continental mantle lithosphere (Maggi et al., 2000), whereas earthquakes certainly occur in oceanic crust and mantle lithosphere (Wiens and Stein, 1983). Maggi et al. (2000) suggest that the strength of continental lithosphere resides in one seismogenic layer within the crust and is controlled by the temperature structure and the amount of water in the crust, similar to oceanic lithosphere. They propose that continental mantle lithosphere is relatively weak and thus aseismic. However, episodes of rifting may affect crustal and mantle rheology. On the other hand, Handy and Brun (2004) show that seismicity is not an indicator of rock strength but argue that seismicity may be used to locate active weak zones within continental lithosphere.

Rifting models at non-volcanic rifted margins of the Atlantic type suggest that the rheology of the continental domain changes during extension (Pérez-Gussinyé and Reston, 2001). With increased stretching, the portion of the crust that becomes brittle increases. Stretching of the lithosphere brings crustal rocks to lower pressure and temperature, and thus the lower part of the crust into brittle domain (Pérez-Gussinyé and Reston, 2001). When the entire crust is brittle, faults can cut through the crust into the mantle and act as fluid pathways, a pre-condition to initiate mantle serpentinisation during rifting (Pérez-Gussinyé and Reston, 2001). The serpentinites create a weak base of the crust, enabling detachment along the CMB and crustal fault block rotation. The serpentine thickness increases with increasing rift duration until the final break-up of the continent (Pérez-Gussinyé and Reston, 2001). The initial conditions and the evolution of the Atlantic-type rifting of old orogens differs from the Ligurian Sea as a back-arc basin where rifting took place during the alpine orogeny. Both margins show similarities and differences: common features are highly weakened continental crust in the ocean–continent transition to a wide and thick basin starting rifting in subaerial conditions; the major difference is that in the Gulf of Lion the continent–ocean transition is probably made of exhumed lower continental crust, while in the Atlantic the upper crust rests directly on top of mantle (Jolivet et al., 2015). We recognise a good relationship between our data and the rifting model of Pérez-Gussinyé and Reston (2001), suggesting that the entire continental crust may have evolved into a more brittle domain during extension. Taking the depth of the C1 events into account this suggests that the mantle was weakened, possibly due to local serpentinisation, down to at least 4 km depth below the CMB. While the high velocity $Vs = 4.7\,km\,s^{-1}$ indicates a generally strong uppermost mantle.

The clustered events discussed here are interpreted to reflect inversion along pre-existing normal faults generated during rifting. Earthquakes within continental mantle lithosphere were also observed in the Gulf of Cadiz, in the southern Iberian old Jurassic mantle lithosphere (Grevemeyer et al., 2016). An explanation could be that during extension, mantle material moves closer to the surface than before stretching, causing mantle temperatures to decrease (Sandiford, 1999). Thus, the mantle in the basin centre might become stronger and more brittle than the surrounding mantle (Sandiford, 1999). Such a scenario is supported by cluster C1 occurring in the uppermost mantle and supporting a low Vp/Vs ratio of 1.72 (Fig. 4b). The crustal structure in the vicinity of clusters C1 and C2 is imaged by the LOBSTER seismic refraction profile p02 (Dannowski et al., 2020). Uncertainties remained for the depth of the base of the sediment layers and the thickness of the crystalline crust, while the depth of the crust–mantle boundary is well imaged. The study provides no indication of a high amount of mantle serpentinisation at its southern end. A high sedimentation rate during rifting (Sage et al., 2011) may have prevented water from penetrating down to the mantle (Rüpke et al., 2013), minimising serpentinisation. However, water may have occasionally reached the mantle, causing serpentinisation around some rift-related faults, weakening the mantle locally (Pérez-Gussinyé and Reston, 2001). Thus, today it may enable the reactivation of rifting-related normal faults as reverse faults.

High heat flow ($> 100\,mW\,m^{-2}$) in the Ligurian Basin (Pasquale et al., 1994) may contradict a cool CMB at the basin centre during rifting. However, recent studies indicate that the Ligurian Basin centre has not yet reached thermal equilibrium since the Oligocene–Miocene rifting process. Thermal modelling for sedimentary basins showed that a combination of a very thick sedimentary cover (> 8 km), extremely low conductive sediments ($< 1.5\,W\,mK^{-1}$), and very shallow and localised crustal radiogenic heat production allow for a present-day temperature maximum at the CMB beneath basin centres (Hansen and Nielsen, 2002). Indeed, the thick sedimentary cover in the centre of the Ligurian Basin (up to 7 km, Schettino and Turco, 2006) might cause thermal blanketing, reducing the lithospheric heat loss, in line with the observed high heat flow values in the basin centre compared to the margins (Béthoux et al., 2008). These effects are also seen in thermal models from the Alps and their forelands, where temperatures at shallow depths (approx. 5 km b.s.l.) in the centre of the Molasse Basin are 20 °C warmer than at the edges (Spooner et al., 2020). Further north-east of our study area, Béthoux et al. (2008) performed

2D thermomechanical modelling to understand the location of seismic activity. They show that the seismogenic zone in the centre of the Ligurian Basin reaches down to ~ 20 km depth. Béthoux et al. (2008) assume oceanic crust in the basin centre and relate the location of earthquakes to contrasts in rheology and the presence of a continent–ocean transfer zone. The events of our observed C1 cluster range in the modelled seismogenic zone for the northern Ligurian basin; the contrast in rheology might be provided by pre-existing rift-related faults reaching the lithospheric mantle.

5 Conclusions

The entire Ligurian Basin is characterised by sparse but widespread micro-earthquakes of magnitude < 3. The ocean-bottom seismometer deployment recorded between June 2017 and February 2018 two earthquake clusters that show thrust faulting mechanisms, supporting a model of inversion of the Ligurian Basin, in which the basin's centre is under compression and stresses are taken up by reactivated faults in the crust and uppermost mantle. Compressional forces are probably related to Africa–Europe plate convergence. The location of the cluster events and their focal mechanisms indicate that they occurred in reactivated pre-existing rift-related structures. Slightly different striking directions of faults in the basin centre compared to faults further east and hence away from the rift basin may reflect the counter-clockwise rotation of the Corsica–Sardinia block. In general, observations of earthquakes in continental mantle lithosphere are rare. A high mantle S-wave velocity of $\mathrm{Vs} = 4.7\,\mathrm{km\,s^{-1}}$ and a low Vp/Vs ratio of 1.72 reveal a strengthening of the crust and uppermost mantle during the Oligocene–Miocene rifting. The observed event cluster indicate local weak zones possibly through local mantle serpentinisation in an otherwise strong lithosphere and support the interpretation that rifting failed in the northern Ligurian Basin. Additional data from an array of more densely spaced OBSs would be needed to obtain a more complete picture of local seismicity in the basin centre.

Appendix A

Here we present additional data plots for data quality and location accuracy of the events that were used for the determination of fault plane solutions: seismic sections (Fig. A1), theoretical and picked arrival times and RMS versus depth (Fig. A2), first motion plots (Fig. A3), and amplitude ratio (Fig. A4).

The software FOCMEC (Snoke, 2003) performs a systematic grid search over all possible the fault plane solutions. FOCMEC determines the polarity of the first motion and calculates the amplitude ratio between S and P waves for each fault plane solutions defined by the angle strike (0–360°), dip (0–90°) and rake (0–180°). Afterwards, these synthetic data (polarity data and amplitude ratio data) are compared with the observed data, and the number of polarity errors and mean deviation of the amplitude rate errors are reported. We selected the 20 best solutions for each event and determined the average fault plane solution. Figure A3 shows the quality of the first motion polarities, and Fig. A4 shows the data fit between the observed and calculated amplitude ratios.

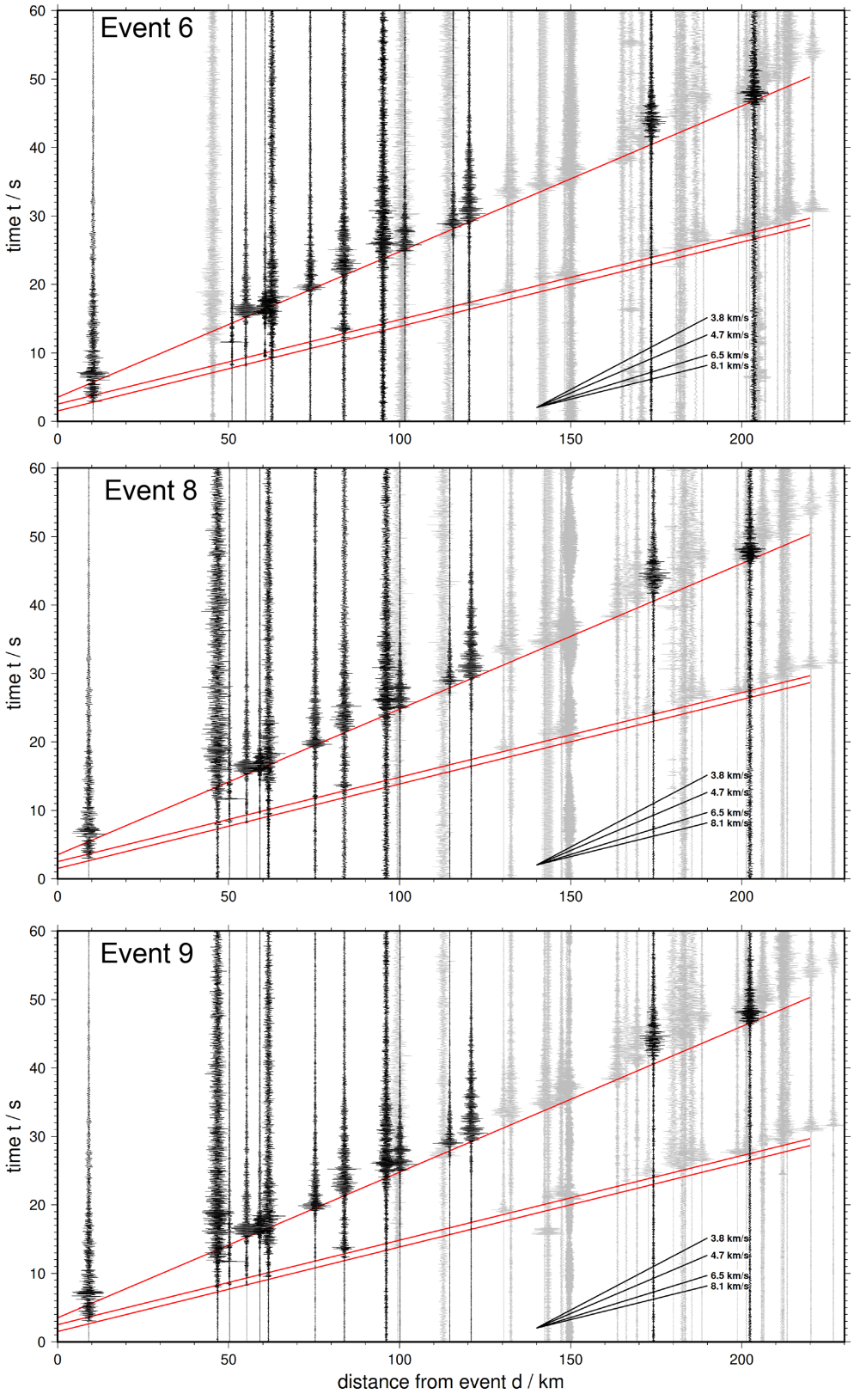

Figure A1. Waveforms observed at stations displayed over offset. Black traces were used for earthquake location. Red lines mark the weak P onset, followed by stronger Ps and S phases. Apparent velocities of $Vp = 8.1\,km\,s^{-1}$ and $Vs = 4.7\,km\,s^{-1}$ observed for the phase onsets (marked with red lines).

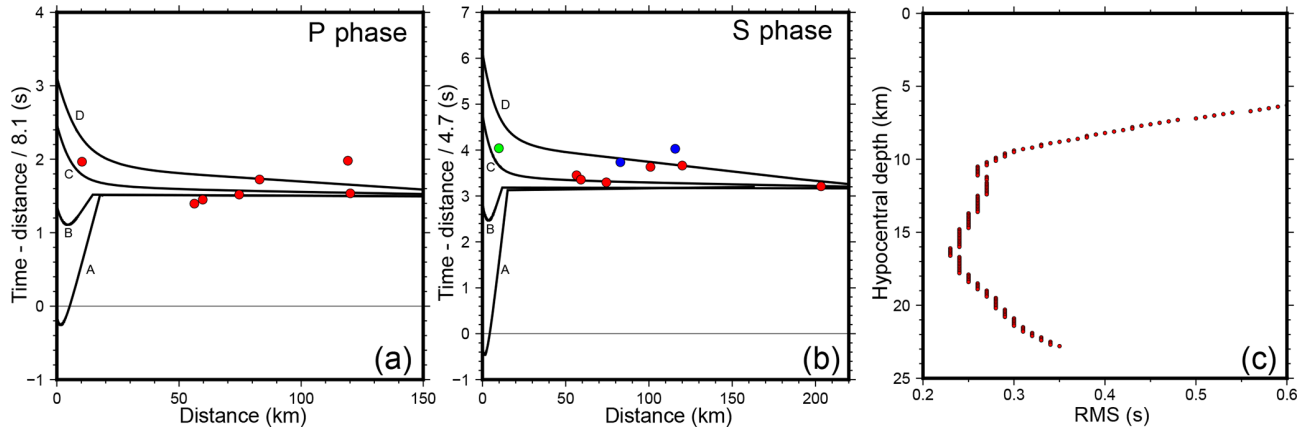

Figure A2. Panels **(a)** and **(b)** show the theoretical (black lines) and observed (coloured dots) first arrival times of the P and S phase for event 2. The colour code displays the picking weight from SEISAN: red – 0 best), green – 1, blue – 2. The theoretical arrival times were calculated for four different hypocentral depths: 6 km for upper crust (A), 10 km for lower crust (B), 16 km (C) and 20 km (D) both for upper mantle. Timings for A, B and D were manually adjusted so that the mantle phase is consistent in all cases. Panel **(c)** displays the uncertainty (RMS versus depth) for the absolute depth estimation of event 2. SEISAN package "rmsdep" was used (Havskov and Ottemoller, 1999, and references therein).

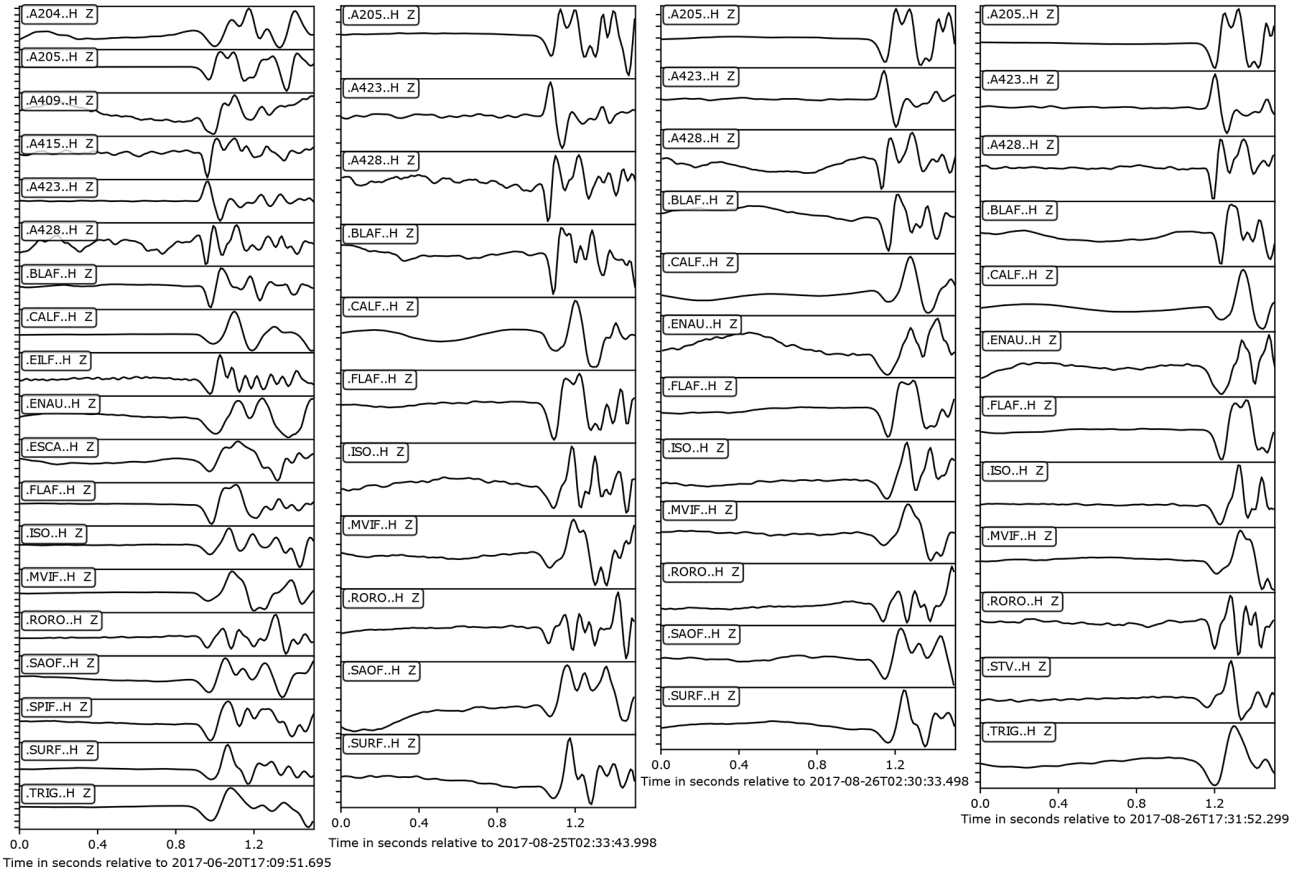

Figure A3. First motion polarities for events 2, 6, 8 and 9 from left to right.

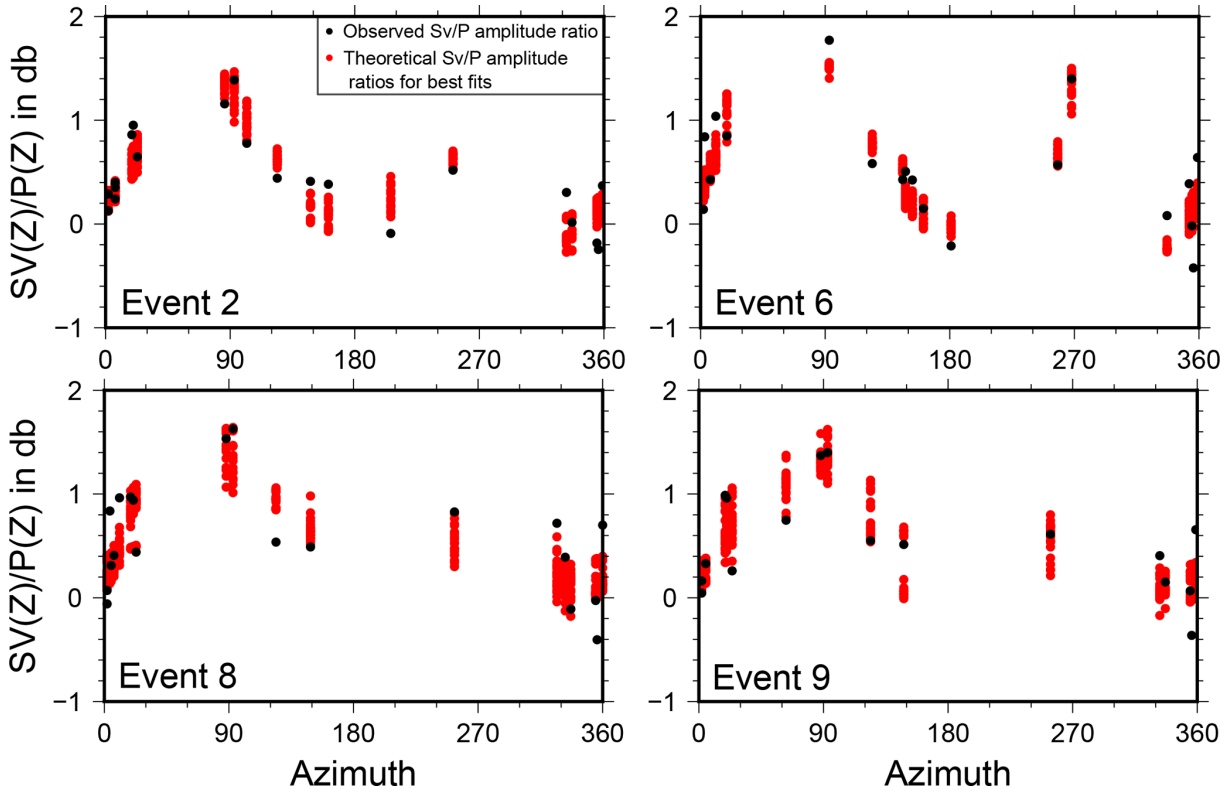

Figure A4. Amplitude ratios of Sv/P for the events 2, 6, 8 and 9. The calculated solutions for the fault plane solutions show a good fit with the observed Sv/P amplitude ratios.

Data availability. Data from the temporary and permanent land stations as well as the OBSs are available through the AlpArray seismic network (Z3, 10.12686/alparray/z3_2015, AlpArray Seismic Network, 2015), the Italian network (IV, https://doi.org/10.13127/SD/X0FXnH7QfY, INGV Seismological Data Centre, 2006), the French RESIF-RLBP network (FR, https://doi.org/10.15778/RESIF.FR, RESIF, 1995), and the Mediterranean MedNet network (MN, https://doi.org/10.13127/SD/fBBBtDtd6q, MedNet Project Partner Institutions, 1990).

Team list. The complete member list of the AlpArray Working Group can be found at http://www.alparray.ethz.ch.

Author contributions. MT carried out data analysis and contributed to the paper. AD wrote the paper and contributed to the data analysis. AD and MT created the figures. IG contributed to the paper with in-depth discussion and editing. HK was PI of the research cruise MSM71 with R/V *Maria S. Merian*. WC was PI of the AlpArray cruise with R/V *Pourquoi Pas?*. HK, DL, IG, MT, AP, WC acquired funding and planned the research concept. HK, AD, FP, MT, DL, AP participated in cruise MSM71 onboard R/V *Maria S. Merian*. WC, FP, AP deployed the AlpArray OBS network on board the R/V *Pourquoi Pas?*.

Competing interests. The authors declare that they have no conflict of interest.

Disclaimer. Publisher's note: Copernicus Publications remains neutral with regard to jurisdictional claims in published maps and institutional affiliations.

Special issue statement. This article is part of the special issue "New insights into the tectonic evolution of the Alps and the adjacent orogens". It is not associated with a conference.

Acknowledgements. We thank the captain and crew of the R/V *Maria S. Merian* (cruise MSM71, 7–27 February 2018) and the R/V *Pourquoi Pas?* (AlpArray cruise, 14–26 June 2017). We thank the cruise participants of both cruises for their efforts. OBS were provided by the DEPAS pool, GEOMAR, and IPGP-INSU pool. The deployment of the German component of the AlpArray seismic network (AASN) was funded by the LOBSTER project that is part of the German Priority Programme SPP2017 4D-MB. The deployment of the French component of the AASN was funded by the AlpArray-FR project of the Agence Nationale de la Recherche (contract ANR-15-CE31-0015). We also thank the AlpArray Seismic Network Team (http://www.alparray.ethz.ch/en/seismic_network/backbone/data-policy-and-citation/, last access: 23 January 2020) and the permanent seismic networks used in this study (FR, IV, and MN). Figures were created using Generic Mapping Tools version 6 (Wessel et al., 2019), ObsPy (Beyreuther et al., 2010), and Inkscape (https://www.inkscape.org, last access: 8 November 2021). We thank Christophe Larroque and Eline Le Breton for their reviews with very constructive comments and suggestions.

Financial support. This research has been supported by the Deutsche Forschungsgemeinschaft (grant nos. TH_2440/1-1, KO_2961/6-1, and LA_2970/4-1) and the Agence Nationale de la Recherche (grant no. ANR-15-CE31- 0015).

The article processing charges for this open-access publication were covered by the GEOMAR Helmholtz Centre for Ocean Research Kiel.

Review statement. This paper was edited by Christian Sue and reviewed by Christophe Larroque and Eline Le Breton.

References

Afilhado, A., Moulin, M., Aslanian, D., Schnürle, P., Klingelhoefer, F., Nouzé, H., Rabineau, M., Leroux, E., and Beslier, M.-O.: Deep crustal structure across a young passive margin from wide-angle and reflection seismic data (The SARDINIA Experiment) – II. Sardinia's margin, B. Soc. Geol. Fr., 186, 331–351, https://doi.org/10.2113/gssgfbull.186.4-5.331, 2015.

AlpArray Seismic Network: AlpArray Seismic Network (AASN) temporary component, AlpArray Working Group, Other/Seismic Network [data set], https://doi.org/10.12686/alparray/z3_2015, 2015.

Alvarez, W., Franks, S. G., and Nairn, A. E. M.: Palaeomagnetism of Plio-Pleistocene Basalts from Northwest Sardinia, Nature Physical Science, 243, 10–11, https://doi.org/10.1038/physci243010a0, 1973.

Bache, F., Olivet, J. L., Gorini, C., Aslanian, D., Labails, C., and Rabineau, M.: Evolution of rifted continental margins: The case of the Gulf of Lions (Western Mediterranean Basin), Earth Planet. Sc. Lett., 292, 345–356, https://doi.org/10.1016/j.epsl.2010.02.001, 2010.

Baroux, E., Béthoux, N., and Bellier, O.: Analyses of the stress field in southeastern France from earthquake focal mechanisms, Geophys. J. Int., 145, 336–348, https://doi.org/10.1046/j.1365-246x.2001.01362.x, 2001.

Béthoux, N.: A closing Ligurian Sea?, Pure Appl. Geophys., 139, 179–194, https://doi.org/10.1007/BF00876326, 1992.

Béthoux, N., Tric, E., Chery, J., and Beslier, M.-O.: Why is the Ligurian Basin (Mediterranean Sea) seismogenic? Thermomechanical modeling of a reactivated passive margin, Tectonics, 27, TC5011, https://doi.org/10.1029/2007TC002232, 2008.

Beyreuther, M., Barsch, R., Krischer, L., Megies, T., Behr, Y., and Wassermann, J.: ObsPy: A Python Toolbox for Seismology, Seismol. Res. Lett., 81, 530–533, https://doi.org/10.1785/gssrl.81.3.530, 2010.

Bigot-Cormier, F., Sage, F., Marc, S., Déverchère, J., Ferrandini, M., Guennoc, P., Popoff, M., and Stéphan, J.-F.: Déformations pliocènes de la marge nord-Ligure (France): les conséquences d'un chevauchement crustal sud-alpin – Pliocene deformation

of the north-Ligurian margin (France): consequences of a south-Alpine crustal thrust, B. Soc. Geol. Fr., 175, 197–211, 2004.

Booth-Rea, G., Ranero, C. R., and Grevemeyer, I.: The Alboran volcanic-arc modulated the Messinian faunal exchange and salinity crisis, Sci. Rep.-UK, 8, 13015, https://doi.org/10.1038/s41598-018-31307-7, 2018.

Bouyahiaoui, B., Sage, F., Abtout, A., Klingelhoefer, F., Yelles-Chaouche, K., Schnürle, P., Marok, A., Déverchère, J., Arab, M., Galve, A., and Collot, J. Y.: Crustal structure of the eastern Algerian continental margin and adjacent deep basin: implications for late Cenozoic geodynamic evolution of the western Mediterranean, Geophys. J. Int., 201, 1912–1938, https://doi.org/10.1093/gji/ggv102, 2015.

Brune, S., Heine, C., Pérez-Gussinyé, M., and Sobolev, S. V.: Rift migration explains continental margin asymmetry and crustal hyper-extension, Nat. Commun., 5, 4014, https://doi.org/10.1038/ncomms5014, 2014.

Burrus, J.: Contribution to a geodynamic synthesis of the Provencal Basin (NorthWestern Mediterranean), Mar. Geol., 55, 247–269, https://doi.org/10.1016/0025-3227(84)90071-9, 1984.

Comas, M., Platt, J. P., Soto, J., and Watts, A.: The origin and Tectonic History of the Alboran Basin: Insights from Leg 161 Results, in: IODP: Preliminary Reports, Ocean Drilling Program, Texas A&M University, College Station, TX 77845-9547, USA, 555–580, https://doi.org/10.2973/odp.proc.sr.161.262.1999, 1999.

Contrucci, I., Nercessian, A., Béthoux, N., Mauffret, A., and Pascal, G.: A Ligurian (Western Mediterranean Sea) geophysical transect revisited, Geophys. J. Int., 146, 74–97, 2001.

Courboulex, F., Larroque, C., Deschamps, A., Kohrs-Sansorny, C., Gélis, C., Got, J. L., Charreau, J., Stéphan, J. F., Béthoux, N., Virieux, J., Brunel, D., Maron, C., Duval, A. M., Perez, J.-L., and Mondielli, P.: Seismic hazard on the French Riviera: observations, interpretations and simulations, Geophys. J. Int., 170, 387–400, https://doi.org/10.1111/j.1365-246X.2007.03456.x, 2007.

Dannowski, A., Kopp, H., Grevemeyer, I., Lange, D., Thorwart, M., Bialas, J., and Wollatz-Vogt, M.: Seismic evidence for failed rifting in the Ligurian Basin, Western Alpine domain, Solid Earth, 11, 873–887, https://doi.org/10.5194/se-11-873-2020, 2020.

Dercourt, J., Zonenshain, L. P., Ricou, L.-E., Kazmin, V. G., Le Pichon, X., Knipper, A. L., Grandjacquet, C., Sbortshikov, I. M., Geyssant, J., Lepvrier, C., Pechersky, D. H., Boulin, J., Sibuet, J.-C., Savostin, L. A., Sorokhtin, O., Westphal, M., Bazhenov, M. L., Lauer, J. P., and Biju-Duval, B.: Geological evolution of the tethys belt from the atlantic to the pamirs since the LIAS, Tectonophysics, 123, 241–315, https://doi.org/10.1016/0040-1951(86)90199-X, 1986.

Dessa, J.-X., Simon, S., Lelievre, M., Beslier, M.-O., Deschamps, A., Béthoux, N., Solarino, S., Sage, F., Eva, E., Ferretti, G., Bellier, O., and Eva, C.: The GROSMarin experiment: three dimensional crustal structure of the North Ligurian margin from refraction tomography and preliminary analysis of microseismic measurements, B. Soc. Geol. Fr., 182, 305–321, https://doi.org/10.2113/gssgfbull.182.4.305, 2011.

Dessa, J.-X., Beslier, M.-O., Schenini, L., Chamot-Rooke, N., Corradi, N., Delescluse, M., Déverchère, J., Larroque, C., Sambolian, S., Canva, A., Operto, S., Ribodetti, A., Agurto-Detzel, H., Bulois, C., Chalumeau, C., and Combe, L.: Seismic Exploration of the Deep Structure and Seismogenic Faults in the Ligurian Sea by Joint Multi Channel and Ocean Bottom Seismic Acquisitions: Preliminary Results of the SEFASILS Cruise, MDPI Geosciences, 10, 108, https://doi.org/10.3390/geosciences10030108, 2020.

Eva, E., Solarino, S., and Spallarossa, D.: Seismicity and crustal structure beneath the western Ligurian Sea derived from local earthquake tomography, Tectonophysics, 339, 495–510, https://doi.org/10.1016/S0040-1951(01)00106-8, 2001.

Eva, E., Malusà, M. G., and Solarino, S.: Seismotectonics at the Transition Between Opposite-Dipping Slabs (Western Alpine Region), Tectonics, 39, e2020TC006086, https://doi.org/10.1029/2020TC006086, 2020.

Faccenna, C., Mattei, M., Funiciello, R., and Jolivet, L.: Styles of back-arc extension in the Central Mediterranean, Terra Nova, 9, 126–130, https://doi.org/10.1046/j.1365-3121.1997.d01-12.x, 1997.

Faccenna, C., Funiciello, F., Giardini, D., and Lucente, P.: Episodic back-arc extension during restricted mantle convection in the Central Mediterranean, Earth Planet. Sc. Lett., 187, 105–116, https://doi.org/10.1016/S0012-821X(01)00280-1, 2001.

Faccenna, C., Piromallo, C., Crespo-Blanc, A., Jolivet, L., and Rossetti, F.: Lateral slab deformation and the origin of the western Mediterranean arcs, Tectonics, 23, TC1012, https://doi.org/10.1029/2002TC001488, 2004.

Finetti, I. R., Boccaletti, M., Bonini, M., Ben, A., Pipan, M., Prizzon, A., and Sani, F.: Lithospheric Tectono-Stratigraphic Setting of the Ligurian Sea–Northern Apennines–Adriatic Foreland from Integrated CROP Seismic Data, in: CROP PROJECT: Deep Seismic Exploration of the Central Mediterranean and Italy, Elsevier B.V., University of Trieste, Trieste, Italy, 119–158, 2005.

Frizon de Lamotte, D., Bezar, B. S., Bracène, R., and Mercier, E.: The two main steps of the Atlas building and geodynamics of the western Mediterranean, Tectonics, 19, 740–761, https://doi.org/10.1029/2000TC900003, 2000.

Gailler, A., Klingelhoefer, F., Olivet, J.-L., and Aslanian, D.: Crustal structure of a young margin pair: New results across the Liguro–Provencal Basin from wide-angle seismic tomography, Earth Planet. Sc. Lett., 286, 333–345, https://doi.org/10.1016/j.epsl.2009.07.001, 2009.

Gattacceca, J., Deino, A., Rizzo, R, Jones, D. S., Henry, B., Beaudoin, B., Valeboin, F.: Miocene rotation of Sardinia: new paleomagnetic and geochronological constraints and geodynamic implications, Earth Planet. Sc. Lett., 258, 359–377, https://doi.org/10.1016/j.epsl.2007.02.003, 2007.

Gómez de la Peña, L., Grevemeyer, I., Kopp, H., Díaz, J., Gallart, J., Booth-Rea, G., Gràcia, E., and Ranero, C. R.: The Lithospheric Structure of the Gibraltar Arc System From Wide-Angle Seismic Data, J. Geophys. Res.-Sol. Ea., 125, e2020JB019854, https://doi.org/10.1029/2020JB019854, 2020.

Grevemeyer, I., Matias, L., and Silva, S.: Mantle earthquakes beneath the South Iberia continental margin and Gulf of Cadiz – constraints from an onshore-offshore seismological network, J. Geodyn., 99, 39–50, https://doi.org/10.1016/j.jog.2016.06.001, 2016.

Gueguen, E., Doglioni, C., and Fernandez, M.: On the post-25 Ma geodynamic evolution of the western Mediterranean, Tectonophysics, 298, 259–269, https://doi.org/10.1016/S0040-1951(98)00189-9, 1998.

Handy, M. R. and Brun, J.-P.: Seismicity, structure and strength of the continental lithosphere, Earth Planet. Sc. Lett., 223, 427–441, https://doi.org/10.1016/j.epsl.2004.04.021, 2004.

Handy, M. R., Schmid, S. M., Bousquet, R., Kissling, E., and Bernoulli, D.: Reconciling plate-tectonic reconstructions of Alpine Tethys with the geological–geophysical record of spreading and subduction in the Alps, Earth-Sci. Rev., 102, 121–158, https://doi.org/10.1016/j.earscirev.2010.06.002, 2010.

Hansen, D. L. and Nielsen, S. B.: Does thermal weakening explain basin inversion?: Stochastic modelling of the thermal structure beneath sedimentary basins, Earth Planet. Sc. Lett., 198, 113–127, https://doi.org/10.1016/S0012-821X(02)00471-5, 2002.

Havskov, J. and Ottemoller, L.: SeisAn Earthquake Analysis Software, Seismol. Res. Lett., 70, 532–534, https://doi.org/10.1785/gssrl.70.5.532, 1999.

Hetényi, G., Molinari, I., Clinton, J., Bokelmann, G., Bondár, I., Crawford, W. C., Dessa, J.-X., Doubre, C., Friederich, W., Fuchs, F., Giardini, D., Gráczer, Z., Handy, M. R., Herak, M., Jia, Y., Kissling, E., Kopp, H., Korn, M., Margheriti, L., Meier, T., Mucciarelli, M., Paul, A., Pesaresi, D., Piromallo, C., Plenefisch, T., Plomerová, J., Ritter, J., Rümpker, G., Šipka, V., Spallarossa, D., Thomas, C., Tilmann, F., Wassermann, J., Weber, M., Wéber, Z., Wesztergom, V., Živčić, M., Abreu, R., Allegretti, I., Apoloner, M.-T., Aubert, C., Besançon, S., Bès de Berc, M., Brunel, D., Capello, M., Čarman, M., Cavaliere, A., Chèze, J., Chiarabba, C., Cougoulat, G., Cristiano, L., Czifra, T., D'Alema, E., Danesi, S., Daniel, R., Dannowski, A., Dasović, I., Deschamps, A., Egdorf, S., Fiket, T., Fischer, K., Funke, S., Govoni, A., Gröschl, G., Heimers, S., Heit, B., Herak, D., Huber, J., Jarić, D., Jedlička, P., Jund, H., Klingen, S., Klotz, B., Kolínský, P., Kotek, J., Kühne, L., Kuk, K., Lange, D., Loos, J., Lovati, S., Malengros, D., Maron, C., Martin, X., Massa, M., Mazzarini, F., Métral, L., Moretti, M., Munzarová, H., Nardi, A., Pahor, J., Péquegnat, C., Petersen, F., Piccinini, D., Pondrelli, S., Prevolnik, S., Racine, R., Régnier, M., Reiss, M., Salimbeni, S., AlpArray Seismic Network Team, AlpArray OBS Cruise Crew, and AlpArray Working Group: The AlpArray Seismic Network: A Large-Scale European Experiment to Image the Alpine Orogen, Surv. Geophys., 39, 1009–1033, https://doi.org/10.1007/s10712-018-9472-4, 2018.

INGV Seismological Data Centre: Rete Sismica Nazionale (RSN), Istituto Nazionale di Geofisica e Vulcanologia (INGV) [data set], Italy, https://doi.org/10.13127/SD/X0FXNH7QFY, 2006.

Inkscape Project: Inkscape [code], available at: https://inkscape.org, 2020.

Jolivet, L. and Faccenna, C.: Mediterranean extension and the Africa-Eurasia collision, Tectonics, 19, 1095–1106, https://doi.org/10.1029/2000TC900018, 2000.

Jolivet, L., Gorini, C., Smit, J., and Leroy, S.: Continental breakup and the dynamics of rifting in back-arc basins: The Gulf of Lion margin: Backarc rift and lower crust extraction, Tectonics, 34, 662–679, https://doi.org/10.1002/2014TC003570, 2015.

Kato, A., Kurashimo, E., Igarashi, T., Sakai, S., Iidaka, T., Shinohara, M., Kanazawa, T., Yamada, T., Hirata, N., and Iwasaki, T.: Reactivation of ancient rift systems triggers devastating intraplate earthquakes, Geophys. Res. Lett., 36, L05301, https://doi.org/10.1029/2008GL036450, 2009.

Larroque, C., Mercier de Lépinay, B., and Migeon, S.: Morphotectonic and fault–earthquake relationships along the northern Ligurian margin (western Mediterranean) based on high resolution multibeam bathymetry and multichannel seismic reflection profiles, Mar. Geophys. Res. 32 (1–2), 163–179, https://doi.org/10.1007/s11001-010-9108-7, 2011.

Larroque, C., Scotti, O., and Ioualalen, M.: Reappraisal of the 1887 Ligurian earthquake (western Mediterranean) from macroseismicity, active tectonics and tsunami modelling: Reappraisal of the 1887 Ligurian earthquake, Geophys. J. Int., 190, 87–104, https://doi.org/10.1111/j.1365-246X.2012.05498.x, 2012.

Larroque, C., Delouis, B., Sage, F., Régnier, M., Béthoux, N., Courboulex, F., and Deschamps, A.: The sequence of moderate-size earthquakes at the junction of the Ligurian basin and the Corsica margin (western Mediterranean): The initiation of an active deformation zone revealed?, Tectonophysics, 676, 135–147, https://doi.org/10.1016/j.tecto.2016.03.027, 2016.

Le Breton, E., Handy, M. R., Molli, G., and Ustaszewski, K.: Post-20 Ma Motion of the Adriatic Plate: New Constraints From Surrounding Orogens and Implications for Crust-Mantle Decoupling: Post-20 Ma Motion of the Adriatic Plate, Tectonics, 36, 3135–3154, https://doi.org/10.1002/2016TC004443, 2017.

Le Breton, E., Brune, S., Ustaszewski, K., Zahirovic, S., Seton, M., and Müller, R. D.: Kinematics and extent of the Piemont–Liguria Basin – implications for subduction processes in the Alps, Solid Earth, 12, 885–913, https://doi.org/10.5194/se-12-885-2021, 2021.

Le Douaran, S., Burrus, J., and Avedik, F.: Deep structure of the north-western Mediterranean Basin: Results of a two-ship seismic survey, Mar. Geol., 55, 325–345, https://doi.org/10.1016/0025-3227(84)90075-6, 1984.

Maffione, M., Speranza, F., Faccenna, C., Cascella, A., Vignaroli, G., and Sagnotti, L.: A synchronous Alpine and Corsica–Sardinia rotation, J. Geophys. Res.-Sol. Ea., 113, B03104, https://doi.org/10.1029/2007JB005214, 2008.

Maggi, A., Jackson, J. A., McKenzie, D., and Priestley, K.: Earthquake focal depths, effective elastic thickness, and the strength of the continental lithosphere, Geology, 28, 495–498, https://doi.org/10.1130/0091-7613(2000)28<495:EFDEET>2.0.CO;2, 2000.

Manchuel, K., Traversa, P., Baumont, D., Cara, M., Nayman, E., and Durouchoux, C.: The French seismic CATalogue (FCAT-17), B. Earthq. Eng., 8, 16. 2227–2251, https://doi.org/10.1007/s10518-017-0236-1, 2017.

Masson, C., Mazzotti, S., Vernant, P., and Doerflinger, E.: Extracting small deformation beyond individual station precision from dense Global Navigation Satellite System (GNSS) networks in France and western Europe, Solid Earth, 10, 1905–1920, https://doi.org/10.5194/se-10-1905-2019, 2019.

Mauffret, A., Frizon de Lamotte, D., Lallemant, S., Gorini, C., and Maillard, A.: E-W opening of the Algerian Basin (Western Mediterranean), Terra Nova, 16, 257–264, https://doi.org/10.1111/j.1365-3121.2004.00559.x, 2004.

MedNet Project Partner Institutions: Mediterranean Very Broadband Seismographic Network (MedNet), Istituto Nazionale di Geofisica e Vulcanologia (INGV) [data set], https://doi.org/10.13127/SD/FBBBTDTD6Q, 1990.

McKenzie, D. P. and Parker, R. L.: The North Pacific: an Example of Tectonics on a Sphere, Nature, 216, 1276–1280, https://doi.org/10.1038/2161276a0, 1967.

Moulin, M., Klingelhoefer, F., Afilhado, A., Aslanian, D., Schnurle, P., Nouzé, H., Rabineau, M., Beslier, M.-O., and Feld, A.: Deep crustal structure across a young passive margin from wide-angle and reflection seismic data (The SARDINIA Experiment) – I. Gulf of Lion's margin, B. Soc. Geol. Fr., 186, 309–330, https://doi.org/10.2113/gssgfbull.186.4-5.309, 2015.

Nicolosi, I., Speranza, F., and Chiappini, M.: Ultrafast oceanic spreading of the Marsili Basin, southern Tyrrhenian Sea: Evidence from magnetic anomaly analysis, Geology, 34, 717–720, https://doi.org/10.1130/G22555.1, 2006.

Nocquet, J.-M.: Present-day kinematics of the Mediterranean: A comprehensive overview of GPS results, Tectonophysics, 579, 220–242, https://doi.org/10.1016/j.tecto.2012.03.037, 2012.

Nocquet, J.-M. and Calais, E.: Geodetic Measurements of Crustal Deformation in the Western Mediterranean and Europe, Pure Appl. Geophys., 161, 661–681, https://doi.org/10.1007/s00024-003-2468-z, 2004.

Pascal, G. P., Mauffret, A., and Patriat, P.: The ocean-continent boundary in the Gulf of Lion from analysis of expanding spread profiles and gravity modelling, Geophys. J. Int., 113, 701–726, https://doi.org/10.1111/j.1365-246X.1993.tb04662.x, 1993.

Pasquale, V., Verdoya, M., and Chiozzi, P.: Types of crust beneath the Ligurian Sea, Terra Nova, 6, 255–266, https://doi.org/10.1111/j.1365-3121.1994.tb00493.x, 1994.

Pérez-Gussinyé, M. and Reston, T. J.: Rheological evolution during extension at nonvolcanic rifted margins: Onset of serpentinization and development of detachments leading to continental breakup, J. Geophys. Res.-Sol. Ea., 106, 3961–3975, https://doi.org/10.1029/2000JB900325, 2001.

Prada, M., Ranero, C. R., Sallarès, V., Zitellini, N., and Grevemeyer, I.: Mantle exhumation and sequence of magmatic events in the Magnaghi–Vavilov Basin (Central Tyrrhenian, Italy): New constraints from geological and geophysical observations, Tectonophysics, 689, 133–142, https://doi.org/10.1016/j.tecto.2016.01.041, 2016.

Rehault, J.-P., Boillot, G., and Mauffret, A.: The Western Mediterranean Basin geological evolution, Mar. Geol., 55, 447–477, https://doi.org/10.1016/0025-3227(84)90081-1, 1984.

RESIF: RESIF-RLBP French Broad-band network, RESIF-RAP strong motion network and other seismic stations in metropolitan France, RESIF – Réseau Sismologique et géodésique Français [data set], https://doi.org/10.15778/resif.fr, 1995.

Rollet, N., Déverchère, J., Beslier, M.-O., Guennoc, P., Réhault, J.-P., Sosson, M., and Truffert, C.: Back arc extension, tectonic inheritance, and volcanism in the Ligurian Sea, Western Mediterranean, Tectonics, 21, 6–1-6–23, https://doi.org/10.1029/2001TC900027, 2002.

Rosenbaum, G., Lister, G., and Duboz, C.: Reconstruction of the tectonic evolution of the Western Mediterranean since the Oligocene, Journal of the Virtual Explorer, 8, 107–130, https://doi.org/10.3809/jvirtex.2002.00053, 2002.

Rüpke, L. H., Schmid, D. W., Perez-Gussinye, M., and Hartz, E.: Interrelation between rifting, faulting, sedimentation, and mantle serpentinization during continental margin formation – including examples from the Norwegian Sea, Geochem. Geophy. Geosy., 14, 4351–4369, https://doi.org/10.1002/ggge.20268, 2013.

Ryan, W. B. F., Carbotte, S. M., Coplan, J. O., O'Hara, S., Melkonian, A., Arko, R., Weissel, R. A., Ferrini, V., Goodwillie, A., Nitsche, F., Bonczkowski, J., and Zemsky, R.: Global Multi-Resolution Topography synthesis, Geochem. Geophy. Geosy., 10, Q03014, https://doi.org/10.1029/2008GC002332, 2009.

Sage, F., Beslier, M. O., Thinon, I., Larroque, C., Dessa, J. X., Migeon, S., Angelier, J., Guennoc, P., Schreiber, D., Michaud, F., Stéphan, J. F., and Sonnette, L.: Structure and evolution of a passive margin in a compressive environment: example of the southwestern Alps-Ligurian basin junction during the Cenozoic, Mar. Petrol. Geol., 28, 1263–1282, https://doi.org/10.1016/j.marpetgeo.2011.03.012, 2011.

Sandiford, M.: Mechanics of basin inversion, Tectonophysics, 305, 109–120, https://doi.org/10.1016/S0040-1951(99)00023-2, 1999.

Schettino, A. and Turco, E.: Plate kinematics of the Western Mediterranean region during the Oligocene and Early Miocene, Geophys. J. Int., 166, 1398–1423, https://doi.org/10.1111/j.1365-246X.2006.02997.x, 2006.

Schmidt-Aursch, M. C. and Haberland, C.: DEPAS (Deutscher Geräte-Pool für amphibische Seismologie): German Instrument Pool for Amphibian Seismology, Journal of large-scale research facilities, 3, 122, https://doi.org/10.17815/jlsrf-3-165, 2017.

Serpelloni, E., Vannucci, G., Pondrelli, S., Argnani, A., Casula, G., Anzidei, M., Baldi, P., and Gasperini, P.: Kinematics of the Western Africa–Eurasia plate boundary from focal mechanisms and GPS data, Geophys. J. Int., 169, 1180–1200, https://doi.org/10.1111/j.1365246X.2007.03367.x, 2007.

Shearer, P. M.: Global seismic event detection using a matched filter on long-period seismograms, J. Geophys. Res., 99, 13713–13725, https://doi.org/10.1029/94JB00498, 1994.

Snoke, J. A.: 85.12 FOCMEC: FOCal MEChanism determinations, in: International Geophysics, Vol. 81, edited by: Lee, W. H. K., Kanamori, H., Jennings, P. C., and Kisslinger, C., Academic Press, 1629–1630, https://doi.org/10.1016/S0074-6142(03)80291-7, 2003.

Speranza, F., Villa, I. M., Sagnotti, L., Florindo, F., Cosentino, D., Cipollari, P., and Mattei, M.: Age of the Corsica–Sardinia rotation and Liguro–Provençal Basin spreading: new paleomagnetic and Ar/Ar evidence, Tectonophysics, 347, 231–251, https://doi.org/10.1016/S0040-1951(02)00031-8, 2002.

Spooner, C., Scheck-Wenderoth, M., Cacace, M., Götze, H.-J., and Luijendijk, E.: The 3D thermal field across the Alpine orogen and its forelands and the relation to seismicity, Glob. Planet. Change, 193, 103288, https://doi.org/10.1016/j.gloplacha.2020.103288, 2020.

Storchak, D. A., Harris, J., Brown, L., Lieser, K., Shumba, B., Verney, R., Di Giacomo, D., and Korger, E. I. M.: Rebuild of the Bulletin of the International Seismological Centre (ISC), part 1: 1964–1979, Geoscience Letters, 4, 32, https://doi.org/10.1186/s40562-017-0098-z, 2017.

van Hinsbergen, D. J. J., Vissers, R. L. M., and Spakman, W.: Origin and consequences of western Mediterranean subduction, rollback, and slab segmentation, Tectonics, 33, 393–419, https://doi.org/10.1002/2013TC003349, 2014.

Waldhauser, F. and Ellsworth, W. L.: A Double-Difference Earthquake Location Algorithm: Method and Application to the Northern Hayward Fault, California, B. Seismol. Soc. Am., 90, 1353–1368, https://doi.org/10.1785/0120000006, 2000.

Wessel, P., Luis, J. F., Uieda, L., Scharroo, R., Wobbe, F., Smith, W. H. F., and Tian, D.: The Generic Mapping

Tools Version 6, Geochem. Geophy. Geosy., 20, 5556–5564, https://doi.org/10.1029/2019GC008515, 2019.

Wiens, D. A. and Stein, S.: Age dependence of oceanic intraplate seismicity and implications for lithospheric evolution, J. Geophys. Res.-Sol. Ea., 88, 6455–6468, https://doi.org/10.1029/JB088iB08p06455, 1983.

Zitellini, N., Ranero, C. R., Loreto, M. F., Ligi, M., Pastore, M., D'Oriano, F., Sallares, V., Grevemeyer, I., Moeller, S., and Prada, M.: Recent inversion of the Tyrrhenian Basin, Geology, 48, 123–127, https://doi.org/10.1130/G46774.1, 2020.

Zoback, M. L.: Stress field constraints on intraplate seismicity in eastern North America, J. Geophys. Res.-Sol. Ea., 97, 11761–11782, https://doi.org/10.1029/92JB00221, 1992.